Bayesian data fusion for water table interpolation: Incorporating a hydrogeological conceptual model in kriging

Luk Peeters,[1] Dominique Fasbender,[2] Okke Batelaan,[1,3] and Alain Dassargues[1,4]

[1] The creation of a contour map of the water table in an unconfined aquifer based on head measurements is often the first step in any hydrogeological study. Geostatistical interpolation methods (e.g., kriging) may provide exact interpolated groundwater levels at the measurement locations but often fail to represent the hydrogeological flow system. A physically based, numerical groundwater model with spatially variable parameters and inputs is more adequate in representing a flow system. Because of the difficulty in parameterization and solving the inverse problem, however, a considerable difference between calculated and observed heads will often remain. In this study the water-table interpolation methodology presented by Fasbender et al. (2008), in which the results of a kriging interpolation are combined with information from a drainage network and a digital elevation model (DEM), using the Bayesian data fusion framework, is extended to incorporate information from a tuned analytic element groundwater model. The resulting interpolation is exact at the measurement locations whereas the shape of the head contours is in accordance with the conceptual information incorporated in the groundwater-flow model. The Bayesian data fusion methodology is applied to a regional, unconfined aquifer in central Belgium. A cross-validation procedure shows that the predictive capability of the interpolation at unmeasured locations benefits from the Bayesian data fusion of the three data sources (kriging, DEM, and groundwater model), compared to the individual data sources or any combination of two data sources.

1. Introduction

[2] A head contour map provides information about the flow direction and gradient of an aquifer system and, in the case of an unconfined aquifer, about the depth of the water table. Such a contour map is used as starting point to gain insight in the groundwater flow system, to evaluate migration of pollutants, to assess vulnerability of an aquifer, and to create conceptual hydrogeological models.

[3] Head observation data, however, are often scarce and irregularly distributed over a study area. To obtain a head contour map based on these data, a number of approaches are available, ranging in complexity from manually drawing contour lines over interpolation to groundwater modeling.

[4] The most straightforward method to create a water table map is to manually create contours on the basis of observation data. This method has the distinct advantage of directly incorporating expert knowledge about the hydro-

geological system under study [*Kresic*, 2006]. A major drawback of manual interpolation is the inherent subjectivity of the method since each expert will have a personal interpretation of the available data and hydrogeological information. A second drawback is the time-consuming nature of the method, especially for large regions and data sets.

[5] The other side of the spectrum of available methods to produce comprehensive and reliable water table maps is physically based, numerical groundwater modeling with spatially distributed parameter and input values. On the basis of the hydrogeological information implemented through the conceptual model, a piezometric map is produced in accordance with the governing groundwater flow equations and mass balance constraints. The major disadvantage of creating such a numerical model to obtain a head contour map is the large amount of hydrogeological data required and the time and the effort needed to create and calibrate the model, whereas, even with a calibrated model, a certain mismatch remains between observed and simulated heads. By increasing the number of parameters and applying optimization algorithms, it is possible to produce one or even several groundwater models without residuals between observed and simulated heads. The decrease in model error is, however, mostly accompanied by a loss of generalization of the model, the ability to adequately simulate a head at unmeasured locations [*Hill and Tiedeman*, 2007]. Numerical groundwater models are therefore seldom created for the sole purpose of creating a groundwater contour map. On the contrary, a contour map is often essential in the

[1]Department of Earth and Environmental Sciences, Katholieke Universiteit Leuven, Heverlee, Belgium.
[2]Centre Eau, Terre et Environnement, Institut National de la Recherche Scientifique, Quebec, Quebec, Canada.
[3]Department of Hydrology and Hydraulic Engineering, Vrije Universiteit Brussels, Brussels, Belgium.
[4]Hydrogéologie et Géologie de l'Environnement, Department of Architecture, Geology, Environment and Constructions, Université de Liege, Liège, Belgium.

conceptualization of boundary conditions for a groundwater model [*Reilly*, 2001].

[6] To create a water table map from groundwater level observations, a wide variety of interpolation techniques are available, including radial basis functions, inverse distance weighting (IDW), and different kriging variants. Recent applications of these methods in the context of water table mapping can be found in work by *Procter et al.* [2006], *Taany et al.* [2009], and *Sun et al.* [2009]. Although these methods honor the data at the measurement locations, they suffer from the same drawbacks, namely, an inadequate representation of the flow system and the occurrence of interpolation artifacts. The inadequate representation of the flow system can be manifested through groundwater levels being interpolated above topography, the lack of flow convergence near draining rivers, or the occurrence of isolated groundwater level depressions in the absence of groundwater extractions. Although these isolated groundwater level depressions can occur naturally, especially in areas with high evapotranspiration rates, in humid and temperate climates, however, isolated groundwater level depressions generally are only linked to groundwater abstraction.

[7] Depending on the method chosen and the implementation of the method, interpolation artifacts can cause both too much smoothing of the surface and abrupt changes in the interpolated surface. In addition, isolated observations can be overemphasized in the interpolation process so that the importance of these observations in the overall interpolation is disproportionately large.

[8] In order to overcome these drawbacks several authors proposed incorporating auxiliary data in the interpolation process. *Kresic* [2006] documents the widely used technique of including dummy points in the interpolation. These artificial points can represent, for instance, a river stage and are included in the interpolation process as extra observations. In doing so the interpolation can be guided as to incorporate a drainage system. *Buchanan and Triantafilis* [2009] improved IDW and ordinary kriging interpolations of groundwater depth using a multiple linear regression of high-resolution geophysical measurements, morphometric information, and observed groundwater levels.

[9] Since groundwater levels are often related to topography in unconfined aquifers [*Haitjema and Mitchell-Bruker*, 2005] and digital elevation models (DEM) are readily available, DEM information can often be used as an auxiliary variable in water table interpolation. *Desbarats et al.* [2002] provide a good overview of different methodologies of incorporating DEM information in a kriging interpolation. Another approach to improving water table interpolation is to incorporate groundwater level calculations on the basis of groundwater-flow equations. The groundwater depth calculated using a linear relationship between groundwater depth and a DEM-derived quantity, the topographic index, as implemented in TOPMODEL, is used by *Desbarats et al.* [2002] as external drift in kriging groundwater depths in Ontario, Canada. *Tonkin and Larson* [2002] incorporate the Theis equation in the calculation of the drift term in kriging in order to account for the effect of pumping on groundwater elevation. *Karanovic et al.* [2009] extend this methodology by using drift terms derived from an analytical element method to include both linear and circular sinks and sources. *Rivest et al.* [2008] adopt a similar approach in which the results of a numerical groundwater

model are used as external drift in the interpolation of a groundwater head field in an earthen dam. *Linde et al.* [2007] use a Bayesian framework to combine self-potential measurements with groundwater level observations to estimate the water table elevation.

[10] The Bayesian data fusion framework was recently used by *Fasbender et al.* [2008] to combine a kriged groundwater contour map with information from a DEM and river network. An empirically derived relationship between groundwater depth and the topography-based penalized distance to the river network is combined with an ordinary kriging of head observation data. Compared to ordinary kriging and cokriging, the resulting interpolation showed an improved accuracy. In addition, the hydrogeological reality was more closely reflected in the interpolated surface, since groundwater flow converged toward draining rivers and the interpolated head was maintained below the topography.

[11] In this study the Bayesian data fusion framework for groundwater head interpolation is extended to implicitly incorporate conceptual hydrogeological information by using a solution to the groundwater flow equations under simplified boundary conditions obtained by the analytic element method.

[12] The methodology is applied to a regional, unconfined, sandy aquifer in Belgium. The performance of the interpolation in terms of predictive capability is assessed using a "leave-one-out" cross-validation procedure in which the predictive capability of the individual data sources (kriging, empirical depth-distance relationship, or groundwater model) and any combination of two data sources is compared to an interpolation using all three data sources.

2. Interpolation Methodology

[13] The goal of any interpolation is to estimate a variable of interest Z_0 at an unsampled location x_0 based on observations $z_S = \{z_1, z_2,...,z_m\}$ at locations $x_S = \{x_1,x_2,...,x_m\}$. In addition to the direct observations of the variable of interest, indirect observations $y = \{y_0,y_1,...,y_n\}$ of secondary data sources Y at locations $\{x_0,x_1, ...,x_n\}$ can be used to refine the interpolation. To apply such a fusion of data, Bayesian approaches have been shown to provide good results in various fields such as image processing, remote sensing, and environmental modeling. An overview of these applications can be found in work by *Bogaert and Fasbender* [2007] and *Fasbender et al.* [2008]. The ensemble Kalman filter data assimilation technique, which is widely applied in atmospheric science [*Ehrendorfer*, 2007], can be considered to be a special case of empirical Bayesian data fusion [*Cressie and Wikle*, 2002].

[14] Within the Bayesian data fusion framework, the interpolation methodology seeks the posterior probability density function (pdf) $f(z_0|y_0)$, the pdf of variable z at unsampled location x_0, given y_0, the secondary information at location x_0. In this study the secondary information consists of a kriging estimate at x_0 based on observations $z_S = \{z_1, z_2,...,z_m\}$ at locations $x_S = \{x_1,x_2,...,x_m\}$, an estimate of z_0 by an empirical depth-distance relationship and an estimate z_0 by an analytical element groundwater model. This section describes the fusion of the different data sources while the details of the individual data sources,

kriging, depth-distance relationship, and analytical element method will be discussed in section 3.

[15] The m secondary data sources at x_0, $Y_\mathbf{0} = (Y_{0,1}, \ldots, Y_{0,m})'$, are related to the variable of interest, Z_0, through an error term E_0:

$$Y_{0,j} = Z_0 + E_{0,j} \;\; \forall j = 1, \ldots, m.$$

Under the assumption of mutual independence of the secondary data sources conditionally to the variable Z_0, *Bogaert and Fasbender* [2007] show that the posterior pdf $f(z_0|y_0)$ can be written in function of the prior pdf of z, $f(z_0)$ and the conditional pdf's $f(z_0|y_{0,i})$ as

$$f(z_0|y_0) \propto \frac{1}{[f(z_0)]^{m-1}} \prod_{j=1}^{m} f(z_0|y_{0,j}). \tag{1}$$

If $f(z_0|z_S)$ denotes the pdf of the variable of interest at location x_0, solely on the basis of observations z_S, obtained through ordinary kriging interpolation of the observation data, if $f(z_0|y_{DEM}(x_0))$ denotes the pdf of z at location x_0 obtained through an empirical depth-distance relationship evaluated at x_0 and if $f(z_0|y_{GW}(x_0))$ is the pdf of z at x_0 from the estimate of the analytical element groundwater model for location x_0, equation (1) can be written as [cf. *Fasbender et al.*, 2008]

$$f[z_0|\, z_S, y_{GW}(x_0), y_{GW}(x_0)] \propto \frac{f(z_0|z_S)}{f(z_0)^2} f[z_0|y_{DEM}(x_0)] f[z_0|y_{GW}(x_0)]. \tag{2}$$

Under the assumption that $f(z_0), f(z_0|z_S), f(z_0|y_{DEM}(x_0))$, and $f(z_0|y_{GW}(x_0))$ are Gaussian distributed, the posterior pdf $f(z_0|z_S, y_{DEM}(x_0), y_{GW}(x_0))$ is also Gaussian. A Gaussian distribution with mean μ and variance σ^2 is given by

$$f(x) = \frac{1}{\sqrt{2\pi}\sigma} \exp\left[-\frac{1}{2\sigma^2}(x-\mu)^2\right] \propto \exp\left(-\frac{1}{2\sigma^2}x^2 + \frac{\mu}{\sigma^2}x\right). \tag{3}$$

Replacing the pdf's on the right-hand side in equation (2) by equation (3) results in the equivalence given by equation (3):

$$
\begin{aligned}
f[z_0|z_S, y_{DEM}(x_0), y_{GW}(x_0)] &\propto \exp\left(\frac{1}{\sigma_0^2}z_0^2 - 2\frac{\mu_0}{\sigma_0^2}z_0\right) \\
&\cdot \exp\left(-\frac{1}{2\sigma_k^2}z_0^2 + \frac{\mu_k}{\sigma_k^2}z_0\right) \times \exp\left(-\frac{1}{2\sigma_{DEM}^2}z_0^2 + \frac{\mu_{DEM}}{\sigma_{DEM}^2}z_0\right) \\
&\cdot \exp\left(-\frac{1}{2\sigma_{GW}^2}z_0^2 + \frac{\mu_{GW}}{\sigma_{GW}^2}z_0\right) \\
&\cdot \propto \exp\left[-\frac{1}{2}\left(\frac{1}{\sigma_k^2} + \frac{1}{\sigma_{DEM}^2} + \frac{1}{\sigma_{GW}^2} - \frac{2}{\sigma_0^2}\right)z_0^2 \right. \\
&\left. + \left(\frac{\mu_k}{\sigma_k^2} + \frac{\mu_{DEM}}{\sigma_{DEM}^2} + \frac{\mu_{GW}}{\sigma_{GW}^2} - 2\frac{\mu_0}{\sigma_0^2}\right)z_0\right].
\end{aligned} \tag{4}
$$

In equation (4) μ_0 and σ_0^2 denote the mean and variance of the observed data set, characterizing the prior pdf, μ_k and σ_k^2 denote the mean and variance of the kriging interpolation, μ_{DEM} and σ_{DEM}^2 denote the mean and variance of the empirical depth-distance relationship, and μ_{GW} and σ^2_{GW} are the mean and variance of the analytic element groundwater model.

[16] Since the conditional probability density function itself is also a Gaussian distribution, the mean and the variance of this pdf. μ_{BDF} and σ^2_{BDF}, respectively, are obtained through equivalence from equation (4):

$$
\begin{cases}
\mu_{BDF} = \left(\dfrac{\mu_k}{\sigma_k^2} + \dfrac{\mu_{DEM}}{\sigma_{DEM}^2} + \dfrac{\mu_{GW}}{\sigma_{GW}^2} - 2\dfrac{\mu_0}{\sigma_0^2}\right)\sigma^2_{BDF} \\[2ex]
\sigma^2_{BDF} = \left(\dfrac{1}{\sigma_k^2} + \dfrac{1}{\sigma_{DEM}^2} + \dfrac{1}{\sigma_{GW}^2} - \dfrac{2}{\sigma_0^2}\right)^{-1}.
\end{cases} \tag{5}
$$

Equation (5) thus provides an elegant and compact formula to estimate a quantity at unmeasured locations by combining a kriging interpolation with different additional data sources, which are exhaustively known in space, with the result of a kriging interpolation.

3. Application

3.1. Study Area

[17] The study area is located in central Belgium where the geology is dominated by the Brussel Sand Formation (Figure 1), one of the main aquifers in Belgium for drinking water production. This Brussel Sand Formation aquifer is of middle Eocene age and consists of a heterogeneous alteration of calcified and silicified coarse sands [*Laga et al.*, 2001]. These sands are deposited on top of a clay formation of early Eocene age, the Kortrijk Formation, which forms the base of the aquifer in the northern part of the study area. In the south, the Kortrijk Formation is locally eroded, and the Brussel Sand Formation is deposited on top of Paleocene sandy silts (Hannut Formation), Cretaceous chalk deposits (Gulpen Formation) and, mainly, Paleozoic basement rocks consisting of weathered and fractured shales and quartzites. On the hilltops, younger sandy formations of late Eocene (Maldegem Formation) to early Oligocene age (St. Huibrechts Hern Formation) cover the Brussel Sand Formation. The St. Huibrechts Hern Formation mainly consists of glauconiferous fine sands. In the north of the study area isolated patches of Oligocene clay (Boom Formation) and Miocene sands (Diest Formation) occur. The entire study area is covered with an eolian loess deposit of the Quaternary age; in the northeast of the study area, these loess deposits are more sandy.

[18] The main river in the study area is the Dijle River, and many of its tributaries have cut through the Brussel Sand Formation during the Quaternary. In most of the valley floors, the Brussel Sand Formation is absent, and the unconfined aquifer is situated in alluvial deposits of the rivers on top of the Kortrijk Formation. These alluvial deposits consist of gravel at the base, covered with an alteration of silt, sand, and peat. In the river valleys, a great number of springs drain the aquifer and provide the base flow for the river Dijle and its tributaries.

[19] The hydraulic conductivity of the Brussel Sand Formation varies between 6.9×10^{-5} and 2.3×10^{-4} m/s because of the heterogeneity of the Eocene aquifer [*Bronders and De Smedt*, 1991]. Locally, in the alluvial gravels, higher conductivities are observed with values as high as 9.3×10^{-4} m/s. Small-scale sedimentary structures have been proven to influence permeability [*Huysmans et al.*, 2008].

[20] Both the Flemish (Puntenlaag grondwatermeetnet, Databank Ondergrond Vlaanderen (in Dutch), 2009, http://dov.vlaanderen.be) and Walloon (Diréction Générale des
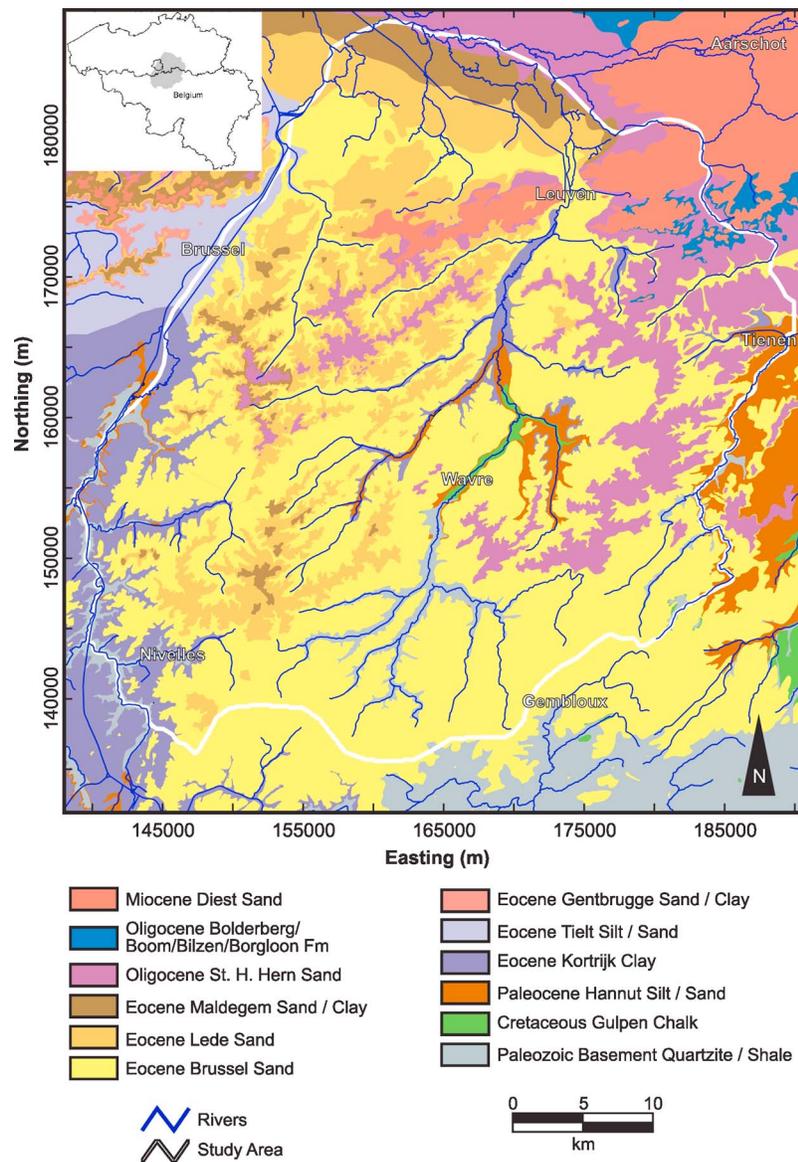
Figure 1. Geological map of the study area (based on data from *Cools et al.* [2006]).

Ressources Naturelles et de l'Environnement, Banque de données 10-sous, 2009, http://carto1.wallonie.be/10SousInt/Default.asp) governments have observation wells installed in the Brussel Sand Formation aquifer to monitor groundwater level fluctuations and groundwater chemistry. The 176 groundwater head observations from these monitoring networks are used for water table interpolation. The locations of the observation wells, the river network, and the topography are indicated in Figure 2.

3.2. Ordinary Kriging

[21] Since the river Dijle drains toward the north and the topography declines in that direction, the head observation data display a clear north-south trend (Figure 3a). A linear trend is fitted to the data and is removed from the data before calculating the experimental variogram (Figure 3b). The experimental variogram is modeled, by fitting in a least squares sense, with a Gaussian variogram with a nugget of 11 m^2, a sill of 308 m^2, and a range of 11,170 m (Figure 3b).

[22] Ordinary kriging with a trend in the y direction, based on the original data and the experimental variogram, is performed on a regular grid with grid cell size of 50 m, having 1140 rows and 1060 columns. In order to incorporate the anisotropy induced by the presence of the draining Dijle River the main axis of the search ellipsoid is oriented N12°E. The radii of the ellipse are 50,000 and 20,000 m with a maximum number of 75 conditioning data. Kriging is performed using the Stanford Geostatistical Modeling Software (S-GeMS) [*Rémy*, 2004]. The kriging interpolation of groundwater head is depicted in Figure 4a, and the associated variance is depicted in Figure 4b.

3.3. Empirical Depth-Distance Relationship

[23] In a first attempt to include additional information in water table spatial mapping within the Bayesian data fusion
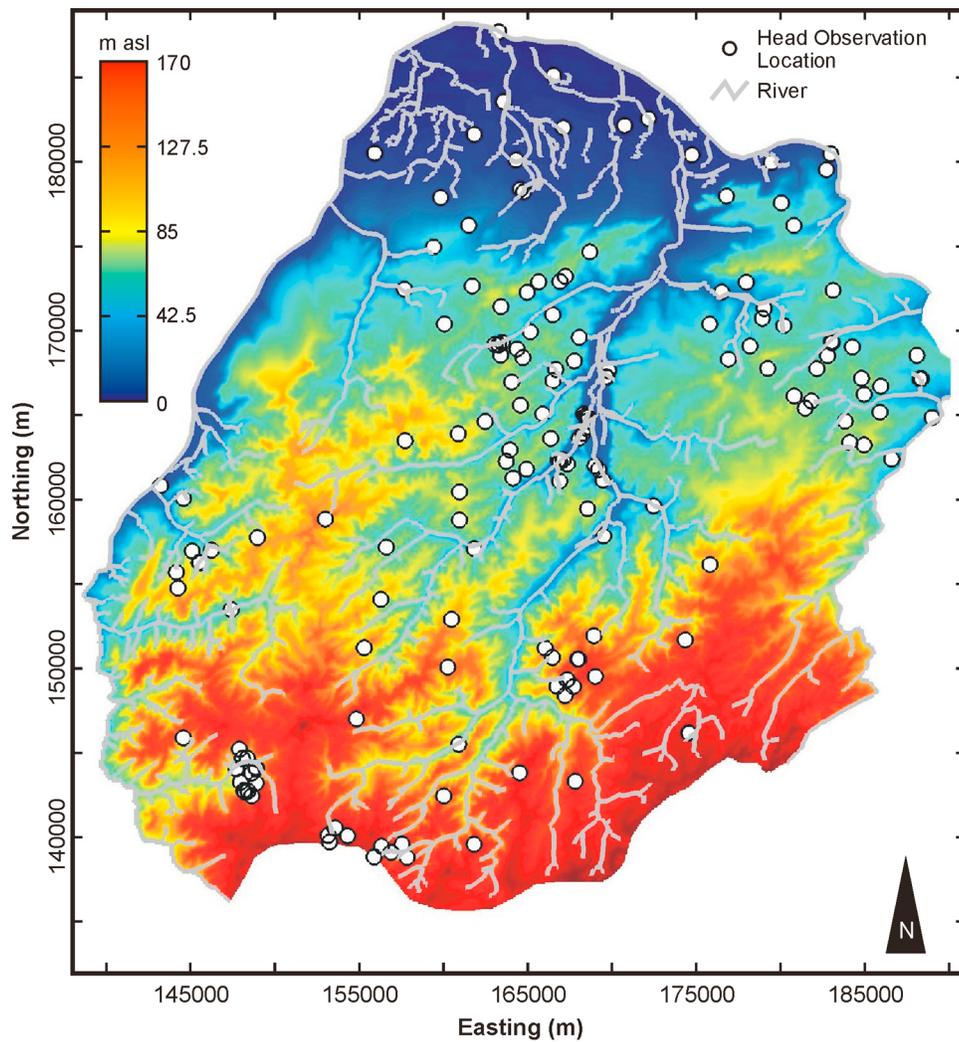
Figure 2. Topography of the study area, river network, and head observation locations.

framework, *Fasbender et al.* [2008] used a digital elevation model and the geometry of the river network. In an aquifer with a draining hydrographic network, water table elevations are expected to be in close proximity to the ground surface near the river network. In an unconfined aquifer, recharge will lead to groundwater mounding in the interfluves. Compared to the rise in elevation of ground level on the interfluves, this mounding generally is rather low,
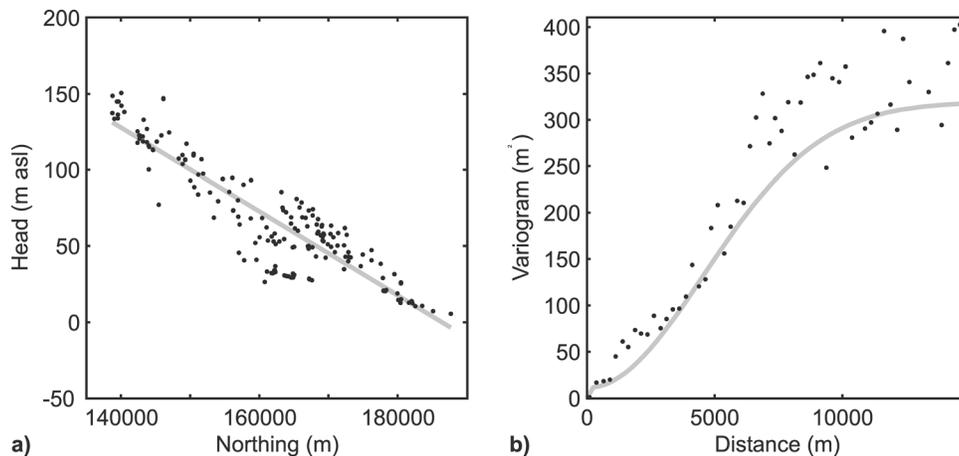
Figure 3. (a) North-south trend identification from observation data and (b) experimental variogram together with the Gaussian variogram model (nugget, 11 m^2; sill, 308 m^2; range, 11170 m).
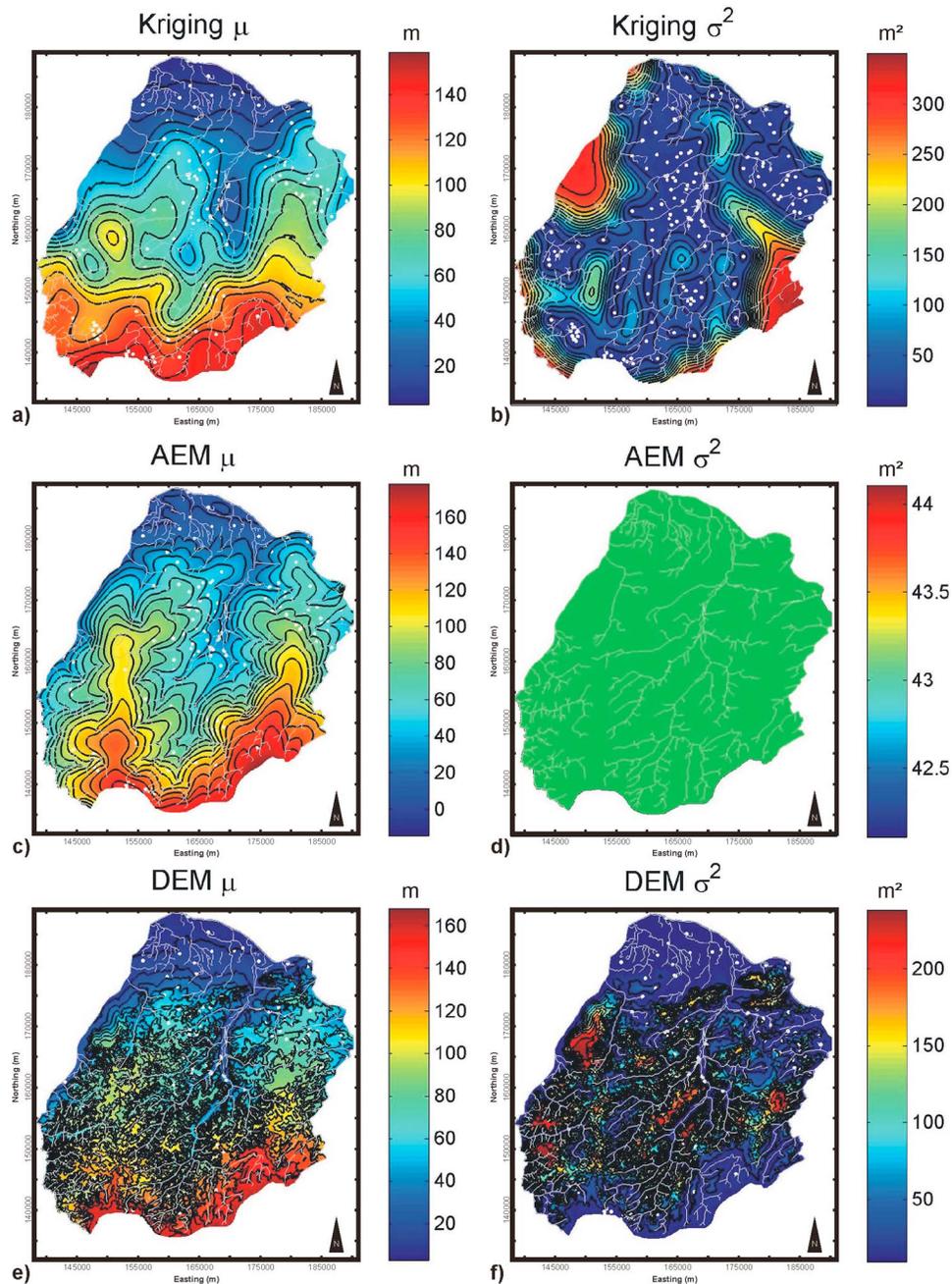
Figure 4. (a) Kriging interpolation, (b) kriging variance, (c) groundwater levels from the analytic element groundwater model, (d) variance of the analytic element groundwater model, (e) groundwater levels estimated with the empirical depth-distance relationship, and (f) variance of the empirical depth-distance estimated groundwater level.

especially in highly conductive aquifers. *Fasbender et al.* [2008] therefore postulate that it is possible to find an empirical function that relates the DEM value to the groundwater level at a certain location on the basis of the distance of the location to the river network. This relationship can be expressed as

$$Z(x_i) = y_{\mathrm{DEM}}(x_i) + E(x_i)$$
$$y_{\mathrm{DEM}}(x_i) = \mathrm{DEM}(x_i) - g[d_{\mathrm{DEM}}(x_i)], \qquad (6)$$

where $Z(x_i)$ is the water table elevation, $y_{\mathrm{DEM}}(x_i)$ is the empirical function, and $E(x_i)$ is a zero-mean random error with a variance σ^2_{DEM}. $\mathrm{DEM}(x_i)$ is the DEM value at location x_i, $d_{\mathrm{DEM}}(x_i)$ is the penalized distance of x_i to the nearest point on the river network, and $g()$ is an increasing nonnegative function. The variance σ^2_{DEM} increases with increasing $d_{\mathrm{DEM}}(x_i)$. This reflects a weakening of the correspondence between water table elevation and ground level elevation as the distance to the river network increases. The distance calculation between x_i and the river network is penalized by using the slope of the terrain. In areas in which
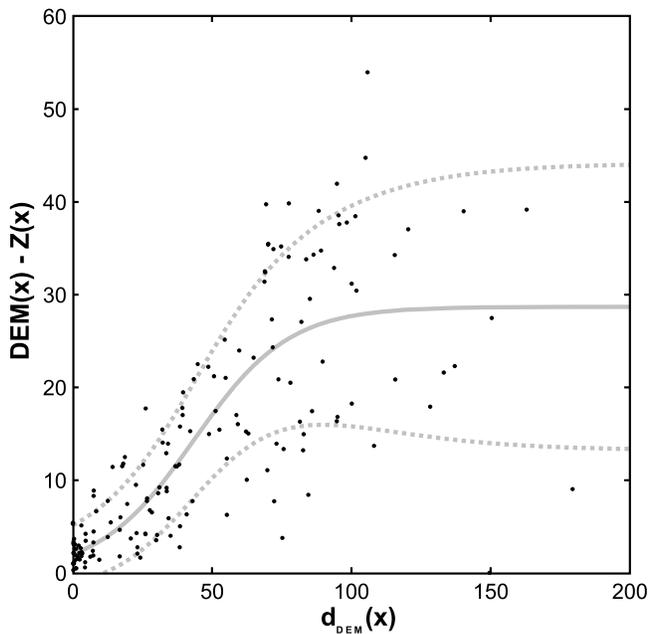
Figure 5. Graph of groundwater depth $DEM(x) - Z(x)$ as a function of penalized distance $d_{DEM}(x)$ to the network. Dots represent the observed pair of values, solid line represents the fitted nonlinear relationship $g()$, and dashed lines represent the 95% symmetric confidence interval based on a Gaussian distribution.

the valleys have steep slopes, a relationship between ground level elevation and water table elevation will not be justified, even if the Euclidean distance to the river network is small. In areas with wide valley floors, on the other hand, water tables will be close to ground level, even if the Euclidean distance to the river network is large. By incorporating the slope in the distance calculation, areas with high ground level fluctuations will have high $d_{DEM}(x_i)$ values and associated high σ^2_{DEM} values, ensuring that these areas get less credit in the Bayesian data fusion (BDF) model.

[24] For each observation location the penalized distance to the nearest point on the hydrographic network is calculated together with the depth of the water table (Figure 5). The depth to the water table clearly increases with increasing penalized distance, especially for relatively small penalized distances. With higher penalized distance, the relationship is not readily apparent. A logistic-like function $g()$ is fitted on the basis of these observations, and the same logistic-like equation is used to model the variance of $E(x_i)$. The choice of a logistic-like function is motivated as it allows an increase of depth with increasing distance while reaching a plateau for larger distances. Using the same type of equation for the variance σ^2_{DEM} ensures that with increasing distance, the variance increases and the influence of the depth-distance relationship on the BDF result decreases. The water table estimate by the empirical depth-distance relationship is shown in Figure 4c, and the associated variance is shown in Figure 4d.

3.4. Analytic Element Groundwater Model

[25] The analytic element method represents aquifer features by points, line sinks, and area sinks, which can be head

or discharge specified to model groundwater flow [*Strack*, 2003]. As the solution to the groundwater flow equations is obtained by superimposing functions of complex potentials representing the aquifer features, there is no need to discretize the flow domain or to specify boundary conditions at the perimeter of the model domain as is needed for finite difference and finite element models [*Strack*, 2003]. Additionally, representing aquifer features by analytic elements facilitates the numerical implementation of the method in object-oriented programming languages [*Bakker and Kelson*, 2009]. Seeing the relative ease of implementing analytic element models, they are popular as a hydrologic screening tool [*Hunt*, 2006]. *Karanovic et al.* [2009] use solutions of analytic elements as drift terms in kriging groundwater heads in an area subject to pumping.

[26] In this study an analytic element groundwater model is created for the Brussel Sand Formation aquifer, using the Tim^{ML} code [*Bakker and Strack*, 2003]. It serves as secondary information in the Bayesian data fusion. The aquifer is represented by a single, unconfined layer with a uniform hydraulic conductivity. The river network shown in Figure 2 is implemented as prescribed head line sinks with a head elevation derived from the DEM. A constant, uniform infiltration of 300 mm/yr [*Batelaan et al.*, 2003] is assigned to the model through a rectangular infiltration area equal to the area spanned by the bounding box of Figure 2. The base of the layer is set to -25 m above sea level (asl) and is assumed to be constant. This is the most simplifying step in the conceptualization of the groundwater flow system, as it is known that the base of the aquifer is irregular, slopes toward the north, and varies between 140 m asl in the south and -70 m asl in the north of the study area [*Cools et al.*, 2006]. The value of -25 m asl is chosen to ensure the base of the aquifer is well below the specified head values at the line sinks throughout the flow domain.

[27] A sensitivity analysis with regard to the base level of the aquifer, hydraulic conductivity, and recharge rate is carried out using UCODE [*Poeter et al.*, 2005]. The composite scaled sensitivity is used to evaluate the parameter sensitivity and is defined as [*Hill and Tiedeman*, 2007]

$$CSS = \sum_{i=1}^{n} \sqrt{\frac{1}{n}\left[\left(\frac{\partial h'_i}{\partial b}\right)|b|\right]^2},\qquad(7)$$

with $\partial h'_i/\partial b$ the sensitivity of the simulated value h'_i associated with the ith observation with respect to parameter b. Using the head observations from section 3.1, the composite scaled sensitivity of the recharge rate and hydraulic conductivity are 0.33 and 0.32, respectively, whereas the value for the base of the aquifer is much lower, 8.1×10^{-3}.

[28] The analytic element model is automatically calibrated by changing the hydraulic conductivity. Recharge rate is not changed, as changes in this parameter are correlated to changes in the hydraulic conductivity parameter. The effect of an increase in recharge rate on hydraulic heads in the aquifer can be countered by increasing the hydraulic conductivity. In a situation as outlined above with an unconfined aquifer with a single hydraulic conductivity and recharge rate, a unique solution to the parameter optimization cannot be obtained by simultaneously changing both parameters [*Hill and Tiedeman*, 2007]. The final hydraulic conductivity obtained after calibration is 1.74×10^{-6} m/s.
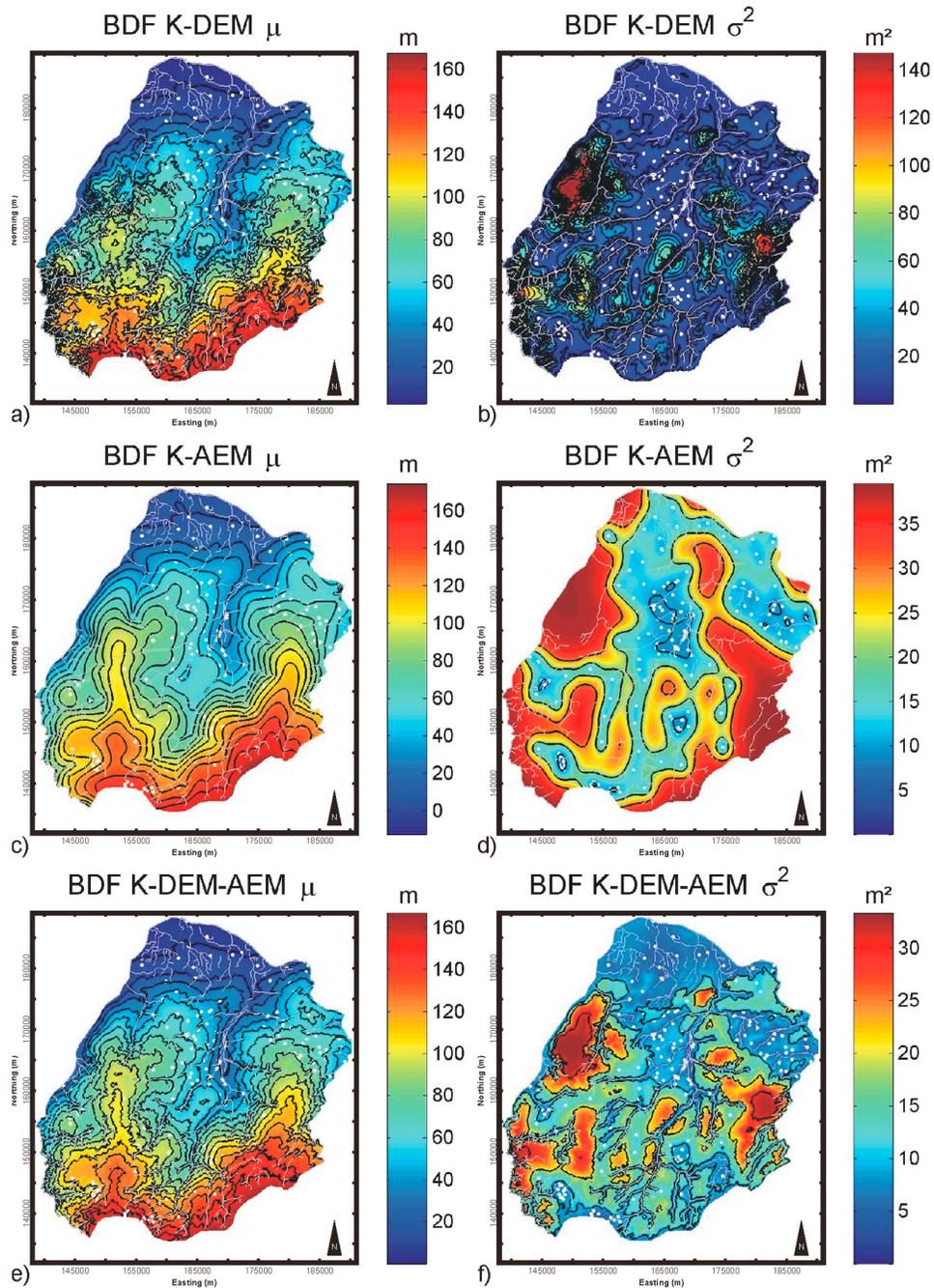
Figure 6. (a) Bayesian data fusion (BDF) of kriging and digital elevation model (DEM), (b) variance of BDF of kriging and DEM, (c) BDF of kriging and analytic element model (AEM), (d) variance of BDF of kriging and AEM, (e) BDF of kriging, DEM, and AEM, and (f) variance of BDF of kriging, DEM, and AEM.

As could be expected, this value is an order of magnitude lower than the values from pumping tests since the base of the aquifer is underestimated.

[29] As for the empirical depth-distance relationship, the estimated groundwater level, $y_{GW}(x_i)$, at a location x_i can be related to the unknown, true groundwater level $Z(x_i)$ by addition of an error term $E(x_i)$ with a zero mean and a variance σ_{GW}^2:

$$Z(x_i) = y_{GW}(x_i) + E(x_i). \tag{8}$$

The variance is chosen to be uniform throughout the model domain, and in order to reflect the capability of the analytic element model at simulating groundwater levels, the mean square error between observed and simulated head is used to model the variance

$$\sigma_{GW}^2 = \frac{1}{N} \sum_{i=1}^{N} \hat{e}_i^2, \tag{9}$$

Table 1. Root-Mean-Square Error and Normalized Root-Mean-Square Error of Cross Validation

Method	RMSE (m)	NRMSE
Kriging	7.24	4.99
AEM	6.57	4.52
DEM	7.37	5.08
BDF kriging, AEM	5.42	3.73
BDF kriging, DEM	4.91	3.39
BDF kriging, AEM and DEM	4.77	3.29

where $\hat{e}_i$ is the estimated error at location x_i and N is equal to 176. The estimated groundwater level using the calibrated analytic element model is shown in Figure 4c, and the associated variance is shown in Figure 4d.

[30] By using more elaborate conceptual models, more closely reflecting the spatial variability in recharge, hydraulic conductivity, and the base of the aquifer, it is not unlikely that the estimated variance will decrease and the influence of the groundwater model on the final BDF interpolation would increase. This would, however, be beyond the scope of the methodology, which aims at providing an interpolation methodology using limited information on the aquifer properties.

3.5. Bayesian Data Fusion

[31] The Bayesian data fusion outlined in section 2 is applied to the study area. In order to assess and to compare the influence of the different additional data sources, three different BDF interpolations are carried out, combining (1) kriging with the empirical depth-distance relationship, (2) kriging with the analytic element groundwater model (AEM), and, finally, (3) kriging with the empirical depth-distance relationship and the analytical element groundwater model. The former can be implemented by using equation (5). For the first interpolation, equation (5) simplifies to

$$\mu_{\text{BDF}} = \left(\frac{\mu_k}{\sigma_k^2} + \frac{\mu_{\text{DEM}}}{\sigma_{\text{DEM}}^2} - \frac{\mu_0}{\sigma_0^2} \right) \sigma_{\text{BDF}}^2$$
$$\sigma_{\text{BDF}}^2 = \left(\frac{1}{\sigma_k^2} + \frac{1}{\sigma_{\text{DEM}}^2} - \frac{1}{\sigma_0^2} \right)^{-1}. \qquad (10)$$

A similar equation can be found for the BDF combining kriging with the analytic element model. The interpolated head obtained through the different BDF interpolations and the associated variances are shown in Figure 6.

[32] To assess the predictive capability of the proposed methodology and to compare the different Bayesian data fusion results to each other and to the individual secondary data sources, a leave-one-out cross validation as outlined by *Chilès and Delfiner* [1999, p. 111] is carried out. For each observation location x_0 groundwater level and associated variance are calculated on the basis of the surrounding observations, without taking into account the observed groundwater level at location x_0. The obtained results are compared to the observed groundwater levels by means of scatterplots and by calculating the root-mean-square error (RMSE) and normalized root-mean-square error (NRMSE) according to

$$\text{RMSE} = \sqrt{\frac{1}{N} \sum_{i=1}^{N} \hat{e}_i^2}$$
$$\text{NRMSE} = \frac{\text{RMSE}}{\max(h_{\text{obs}}) - \min(h_{\text{obs}})}, \qquad (11)$$

with $\hat{e}_i$ the estimated error at location x_i and N the number of observations h_{obs}. The calculated RMSE and NRMSE are given in Table 1.

[33] For the kriging interpolation, cross validation consisted of estimating groundwater level and variance at observation location x_i without taking into account the groundwater level observation at x_i. For the cross validation of the empirical depth-distance relationship, the relationship and associated variance are estimated without using the observation at x_i. As such, the analytic element model does not use the observations to estimate groundwater level. The calculated groundwater level at location x_i is therefore used as a cross-validation value. The associated variance, however, obtained through equation (9) is calculated without using the groundwater level observation at x_i. The cross validation of the three BDF interpolations at x_i is obtained by plugging the groundwater level values and variance at x_i values from the cross validation of the secondary information sources into equations (5) and (10).

4. Discussion

[34] From Figure 4a it is apparent that kriging produces a smoothly varying water table contour map with depressions situated in the vicinity of the major rivers (Figure 2). The variance map (Figure 4b), however, shows the irregular distribution of observation points and the resulting low variance in the central area with a high observation density, whereas the eastern and western borders, regions scarce of data, are characterized by a high variance. This variance map helps to explain a number of interpolation artifacts present in Figure 4a. In regions in the vicinity of (x,y) coordinates (170000,165000) and (x,y) coordinates (147000,145000), isolated depressions are interpolated. Such depressions should only occur in a groundwater level contour map if a groundwater extraction, by pumping wells or by evaporation through a pond, is present. In this aquifer system, however, the depression represents a part of the flow convergence caused by the draining influence of the river network. In regions with low data density, like the southeast around (x,y) coordinates (180000,150000), the search ellipsoid will not contain enough observation points to produce a reliable interpolation. The contour lines can therefore locally have a jagged appearance although a Gaussian variogram model is used. In a water table interpolation, jagged contour lines should not appear since groundwater levels are to be considered a spatially smoothly varying quantity. The cross validation (Figure 7a) shows that the residuals are centered on zero, and, although some outlying residuals show a considerable departure from zero, the root-mean-square error is only 7.24 m and the normalized root-mean-square error is 4.99%.

[35] The RMSE and NRMSE of the calibrated analytical element groundwater model are comparable to the result of kriging (Table 1). The scatterplot of observed versus calculated values (Figure 7b), however, shows that although the number of very large residuals is smaller compared to kriging, the spread of the residuals around zero is larger. In the groundwater level map (Figure 4c) the difference between the analytic element groundwater model and kriging is clearly visible. The groundwater map shows the draining influence near the rivers and the groundwater mounding due to groundwater recharge in the interfluves. Although the shape of the water table more closely reflects
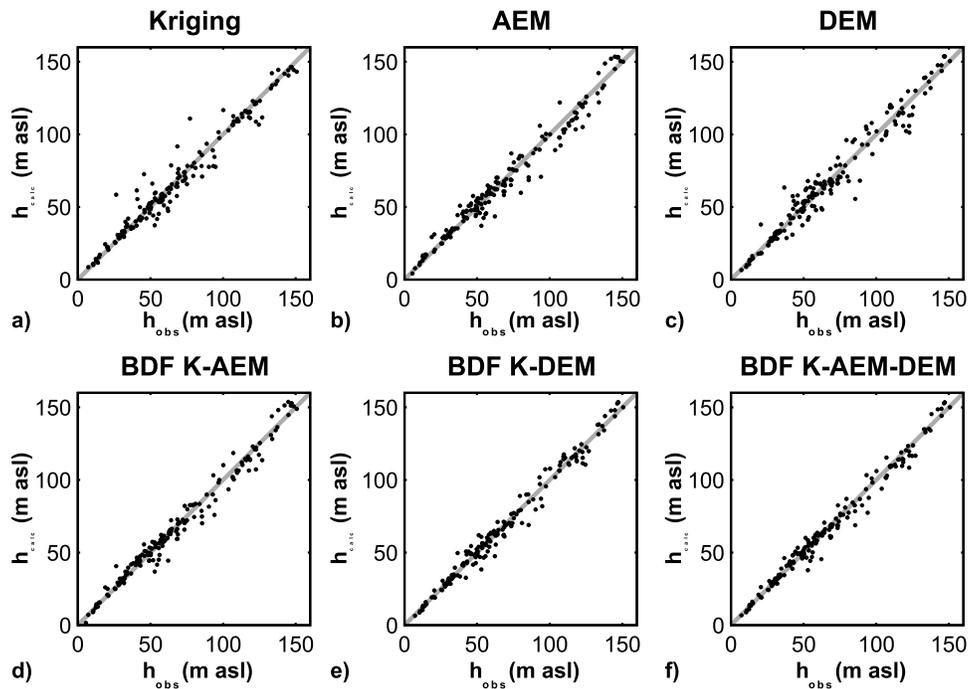
Figure 7. Cross-validation results. Observed values versus calculated values by (a) kriging, (b) analytic element (AEM) groundwater model, (c) empirical depth-distance relationship, (d) BDF of kriging and AEM, (e) BDF of kriging and DEM, and (f) BDF of kriging, AEM, and DEM.

the hydrogeological information available for the aquifer system, locally sizeable differences between observed and calculated groundwater levels exist.

[36] The groundwater level estimated by the empirical depth-distance relationship can be considered a subdued replica of topography. On the interfluves, the contour lines are irregular, reflecting variations in the DEM, whereas the groundwater levels at these locations are expected to be rather smooth and gradually changing. These zones are assigned a high variance, as they have a large penalized distance to the river network. In zones with a low relief, like the alluvial plains and the northern part of the study area, groundwater levels are estimated close to the ground surface. The predictive abilities of this empirical model (Table 1 and Figure 7c) appear to be only slightly lower than those of kriging interpolation.

[37] The first result of Bayesian data fusion interpolation is the combination of the kriging interpolation with the estimate from the empirical depth-distance relationship, as already implemented by *Fasbender et al.* [2008]. In the areas with low relief smooth contour lines are produced (Figure 6a), and the drainage network is incorporated into the interpolation result. On the interfluves, however, the contour lines are often highly irregular with numerous small isolated groundwater mounds and depressions. The variance map (Figure 6b) shows that the zones with high data density and low relief have low variance values. These values increase rapidly, however, in zones with considerable relief and low data density. The scatterplot of cross-validation results (Figure 7e) and the RMSE value of 4.91 m (Table 1) indicate a marked improvement in predictive capability compared to the individual additional data sources.

[38] The BDF interpolation combining kriging with the analytic element groundwater model (Figure 6c) shows a

contour map that is similar to the contour map of the analytic element groundwater model (Figure 4c). The AEM groundwater model, however, appears to locally overestimate the amount of groundwater mounding in the interfluves. This is remediated in zones with high data density, such as around x,y coordinates (170000,170000), by the higher weight of the kriging in the interpolation. In zones with low data density, the effect of the drainage network on the contour lines of groundwater elevation is clearly apparent. Where data density is high in the vicinity of a river, it is possible that kriging dominates the interpolation, as can be seen near x,y coordinates (145000,150000) and x,y coordinates (160000,160000). As the AEM groundwater model is characterized by a uniform variance, the variance of BDF of the kriging and AEM (Figure 6d) is a scaled replica of the kriging variance (Figure 4b). The RMSE of this interpolation, 5.42 m, is slightly higher than the RMSE of the BDF of kriging and the depth-distance relationship. The main reason for the higher RMSE is the presence of higher residuals for the observations with groundwater levels above 100 m, whereas for observations below 100 m the BDF of kriging and AEM has lower residuals.

[39] The ultimate interpolation combines the three data sources, kriging, depth-distance relationship, and AEM groundwater model (Figure 6e). The general shape of the contour lines is largely influenced by the analytic element model. Locally, the influence of the other data sources is apparent, especially in zones with high data density (kriging) and near the river network (depth-distance relationship). The influence of the depth-distance relationship can also be seen on the interfluves through the irregularities in the contour lines, arising from the DEM fluctuations. The variance of the BDF in Figure 6f benefits clearly from incorporating the empirical depth-distance relationship. The

cross-validation results, i.e., both the scatterplot and the RMSE value, show that the combination of the three data sources has the highest predictive capabilities.

5. Conclusions

[40] The water table interpolation methodology introduced by *Fasbender et al.* [2008], based on the Bayesian data fusion framework [*Bogaert and Fasbender*, 2007], is further extended to incorporate conceptual hydrogeological information through groundwater head calculation based on an AEM groundwater model.

[41] The methodology is applied to a sandy aquifer in Belgium using a limited number of head observations. The Bayesian data fusion methodology is used to combine kriging with an estimate of groundwater level by an empirical depth-distance relationship and a groundwater level estimate from an automatically calibrated analytic element model.

[42] Combining kriging with the empirical depth-distance relationships produces reliable results in areas that have low relief and are close to the river network. The estimate in zones scarce of data farther away from the river network benefits from combining the kriging with the analytic element groundwater model. Combining the three sources of data results in a groundwater level interpolation with a high level of predictive capabilities as shown through the leave-one-out cross validation, albeit the shape of the contour lines in the interfluves can be debatable because of the presence of irregularities arising from the contribution of the depth-distance relationship.

[43] The interpolation methodology presented and applied in this paper shows that using different sources of data in groundwater interpolation within the Bayesian data fusion framework, even with limited data, makes it possible to produce an accurate water table contour map incorporating conceptual hydrogeological information.

References

Bakker, M., and V. A. Kelson (2009), Writing analytic element programs in Python, *Ground Water*, 47(6), 828–834, doi:10.1111/j.1745-6584.2009.00583.x.

Bakker, M., and O. D. L. Strack (2003), Analytic elements for multiaquifer flow, *J. Hydrol.*, 271(1–4), 119–129.

Batelaan, O., F. De Smedt, and L. Triest (2003), Regional groundwater discharge: Phreatophyte mapping, groundwater modeling and impact analysis of land-use change, *J. Hydrol.*, 275(1–2), 86–108, doi:10.1016/S0022-1694(03)00018-0.

Bogaert, P., and D. Fasbender (2007), Bayesian data fusion in a spatial prediction context: A general formulation, *Stochastic Environ. Res. Risk Assess.*, 21(6), 695–709, doi:10.1007/s00477-006-0080-3.

Bronders, J., and F. De Smedt (1991), Geostatistische analyse van de hydraulische geleidbaarheid van watervoerende lagen in Midden-België (Geostatistical analysis of hydraulic conductivity of the aquifers in central Belgium), *Water*, 59(4), 127–132.

Buchanan, S., and J. Triantafilis (2009), Mapping water table depth using geophysical and environmental variables, *Ground Water*, 47(1), 80–96, doi:10.1111/j.1745-6584.2008.00490.

Chilès, J.-P., and P. Delfiner (1999), *Geostatistics: Modeling spatial uncertainty*, John Wiley, New York.

Cools, J., Y. Meyus, S. T. Woldeamlak, O. Batelaan, and F. De Smedt (2006), Large-scale GIS-based hydrogeological modelling of Flanders: A tool for groundwater management, *Environ. Geol.*, 50(8), 1201–1209, doi:10.1007/s00254-006-0292-3.

Cressie, N., and C. K. Wikle (2002), Space-time Kalman filter, in *Encyclopedia of Environmetrics*, vol. 4, edited by A. H. El-Shaarawi and W. W. Piegorsch, pp. 2045–2049, JohnWiley, New York.

Desbarats, A. J., C. E. Logan, M. J. Hinton, and D. R. Sharpe (2002), On the kriging of water table elevations using collateral information from a digital elevation model, *J. Hydrol.*, 255(1–4), 25–38, doi:10.1016/S0022-1694(01)00504-2.

Ehrendorfer, M. (2007), A review of issues in ensemble-based Kalman filtering, *Meteorol. Z.*, 16(6), 795–818, doi:10.1127/0941-2948/2007/0256.

Fasbender, D., L. Peeters, P. Bogaert, and A. Dassargues (2008), Bayesian data fusion applied to water table spatial mapping, *Water Resour. Res.*, 44, W12422, doi:10.1029/2008WR006921.

Haitjema, H. M., and S. Mitchell-Bruker (2005), Are water tables a subdued replica of the topography?, *Ground Water*, 43(6), 781–786, doi:10.1111/j.1745-6584.2005.00090.

Hill, M. C., and C. R. Tiedeman (2007), *Effective Groundwater Model Calibration*, John Wiley, New York.

Hunt, R. J. (2006), Groundwater modeling applications using the analytic element method, *Ground Water*, 44(1), 5–14, doi:10.1111/j.1745-6584.2005.00143.x.

Huysmans, M., L. Peeters, G. Moermans, and A. Dassargues (2008), Relating small-scale sedimentary structures and permeability in a cross-bedded aquifer, *J. Hydrol.*, 361(1–2), 41–51, doi:10.1016/j.jhydrol.2008.07.047.

Karanovic, M., M. Tonkin, and D. Wilson (2009), KT3D_H2O: A program for kriging water level data using hydrologic drift terms, *Ground Water*, 47(4), 580–586, doi:10.1111/j.1745-6584.2009.00565.x.

Kresic, N. (2006), *Hydrogeology and Groundwater Modeling*, 2nd ed., CRC Press, Boca Raton, Fla.

Laga, P., S. Louwye, and S. Geets (2001), Paleogene and neogene lithostratigraphic units (Belgium), *Geol. Belg.*, 4(1–2), 135–152.

Linde, N., A. Revil, A. Bolève, C. Dagès, J. Castermant, B. Suski, and M. Voltz (2007), Estimation of the water table throughout a catchment using self-potential and piezometric data in a Bayesian framework, *J. Hydrol.*, 334(1–2), 88–98, doi:10.1016/j.jhydrol.2006.09.027.

Poeter, E., M. C. Hill, E. Banta, S. Mehl, and S. Christensen (2005), UCODE_2005 and six other computer codes for universal sensitivity analysis, calibration and uncertainty evaluation, U.S. Geol. Surv. Tech. Methods, 6-A11, 283 pp.

Procter, C., L. Comber, M. Betson, D. Buckley, A. Frost, H. Lyons, A. Riding, and K. Voyce (2006), Identifying crop vulnerability to groundwater abstraction: Modeling and expert knowledge in a GIS, *J. Environ. Manage.*, 81(3), 296–306, doi:10.1016/j.jenvman.2006.01.016.

Reilly, T. E. (2001), System and boundary conceptualization in groundwater flow simulation, *U.S. Geol. Surv. Tech. Water Resour. Invest.*, Book 3, Chap. B8.

Rémy, N. (2004), *S-GeMS: Geostatistical Earth Modelling Software: User's Manual*, Stanford Univ., Stanford, Calif.

Rivest, M., D. Marcotte, and P. Pasquier (2008), Hydraulic head field estimation using kriging with an external drift: A way to consider conceptual model information, *J. Hydrol.*, 361(3–4), 349–361, doi:10.1016/j.jhydrol.2008.08.006.

Strack, O. D. L. (2003), Theory and applications of the analytic element method, *Rev. Geophys.*, 41(2), 1005, doi:10.1029/2002RG000111.

Sun, Y., S. Kang, F. Li, and L. Zhang (2009), Comparison of interpolation methods for depth to groundwater and its temporal and spatial variations in the Minqin oasis of northwest China, *Environ. Modell. Software*, 24(10), 1163–1170, doi:10.1016/j.envsoft.2009.03.009.

Taany, R., A. Tahboub, and G. Saffarini (2009), Geostatistical analysis of spatiotemporal variability of groundwater level fluctuations in Amman-Zarqa basin, Jordan: A case study, *Environ. Geol.*, 57(3), 525–535, doi:10.1007/s00254-008-1322-0.

Tonkin, M. J., and S. P. Larson (2002), Kriging water levels with a regional-linear and point-logarithmic drift, *Ground Water*, 40(2), 185–193.

O. Batelaan, Department of Hydrology and Hydraulic Engineering, Vrije Universiteit Brussels, Pleinlaan 2, B-1050 Brussels, Belgium.

A. Dassargues, Hydrogéologie et Géologie de l'Environnement, Department of Architecture, Geology, Environment and Constructions, Université de Liege, B.52/3 Sart-Tilman, B-4000 Liège, Belgium.

D. Fasbender, Centre Eau, Terre et Environnement, Institut National de la Recherche Scientifique, 490 de la Couronne, Quebec, QC G1K 9A9, Canada.

L. Peeters, Department Earth and Environmental Sciences, Katholieke Universiteit Leuven, Celestijnenlaan 200E bus 2408, B-3001 Heverlee, Belgium. (luk.peeters@csiro.au)